Coplanar cavity for strong coupling between photons and magnons in van der Waals antiferromagnet

Supriya Mandal, Lucky N. Kapoor, Sanat Ghosh, John Jesudasan, Soham Manni, A. Thamizhavel, Pratap Raychaudhuri, Vibhor Singh, and Mandar M. Deshmukh

View Online   Export Citation   CrossMark

ARTICLES YOU MAY BE INTERESTED IN

Coplanar cavity for strong coupling between photons and magnons in van der Waals antiferromagnet

Supriya Mandal,[1] (iD) Lucky N. Kapoor,[1] (iD) Sanat Ghosh,[1] (iD) John Jesudasan,[1] (iD) Soham Manni,[1,2] (iD)
A. Thamizhavel,[1] (iD) Pratap Raychaudhuri,[1] (iD) Vibhor Singh,[3,a] (iD) and Mandar M. Deshmukh[1,a] (iD)
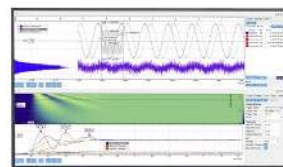
AFFILIATIONS

[1]Department of Condensed Matter Physics and Materials Science, Tata Institute of Fundamental Research, Homi Bhabha Road, Mumbai 400005, India
[2]Department of Physics, Indian Institute of Technology Palakkad, Palakkad 678557, India
[3]Department of Physics, Indian Institute of Science, Bangalore 560012, India

[a]Authors to whom correspondence should be addressed: v.singh@iisc.ac.in and deshmukh@tifr.res.in

ABSTRACT

We investigate the performance of niobium nitride superconducting coplanar waveguide resonators toward realizing hybrid quantum devices with magnon-photon coupling. We find internal quality factors $\sim 20\,000$ at 20 mK base temperature, in zero magnetic field. We find that by reducing film thickness below 100 nm, an internal quality factor greater than 1000 can be maintained up to a parallel magnetic field of ~ 1 T and a perpendicular magnetic field of ~ 100 mT. We further demonstrate strong coupling of microwave photons in these resonators with magnons in chromium trichloride, a van der Waals antiferromagnet, which shows that these cavities serve as a good platform for studying magnon-photon coupling in 2D magnonics based hybrid quantum systems. We demonstrate strong magnon-photon coupling for both optical and acoustic magnon modes of an antiferromagnet.

Published under license by AIP Publishing. https://doi.org/10.1063/5.0029112

Superconducting coplanar waveguide (SCPW) resonators are of interest as elements of architecture for hybrid quantum systems and quantum computation related studies. The two dimensional (2D) structure, scalability, and control over impedance across varying length scales for SCPW provide a natural way to couple them with various mesoscopic systems. They have been used for making kinetic inductance detectors[1] and parametric amplifiers[2,3] and have been coupled to superconducting qubits,[4] nano-mechanical resonators,[5,6] spin ensembles,[7-11] and quantum dots.[12,13] They have become an important component for realizing hybrid quantum devices.

For application of SCPW resonators in hybrid quantum devices involving electron spin resonance (ESR) systems,[9,14-16] nitrogen vacancy (NV) centers,[7,8] and different topological systems,[17-19] performance under magnetic field is additionally required. Furthermore, with the advent of 2D magnetic materials[20] and possibility to utilize their unique properties in hybrid quantum designing schemes, ~ 100 mT magnetic field in arbitrary directions is required. This additional requirement for the SCPW resonators necessitates the use of type-II superconductors having high upper critical magnetic field

(H_{C2}) like Mo–Re, TiN, Nb–Ti–N, and NbN.[21-25] In the presence of magnetic field, flux vortices are generated in these materials which cause dissipative vortex motion in the presence of high frequency oscillatory currents. Moreover, reduction in Cooper pairs due to the formation of normal cores of the vortices causes an increase in kinetic inductance which cause a decrease in resonance frequency.[26] Control over this kind of vortex induced dissipation can be achieved through the introduction of pinning sites to trap the vortices which can either be done by utilizing intrinsic disorder[27] or by fabricating artificial pinning sites.[28-30]

Niobium nitride (NbN) is a disordered type-II superconductor with a high transition temperature ($T_C \approx 16.8$ K), high upper critical magnetic field ($H_{C2} \approx 15$ T), small coherence length (≈ 5 nm), and large penetration depth (≈ 250 nm).[31-33] NbN thin films of varying thicknesses with moderately high T_C can be realized, which are also stable in ambient condition and robust with respect to thermal cycling from room temperature to cryogenic temperatures. Another interesting property of NbN is that its T_C depends mainly on the carrier density (and not disorder) for samples with $T_C > 10$ K.[31] This makes

NbN a potential candidate for reducing dissipation due to vortices by utilizing inherent disorder.

In this work, we fabricate and probe the properties of NbN SCPW resonators. Traditionally, SCPW resonators are fabricated by careful substrate surface preparation followed by the deposition of superconducting films. Subsequently, etching processes are used to pattern the resonator. Here, we intentionally use a simple liftoff based fabrication process. The motivation behind this approach is twofold: (a) it helps to establish baseline properties and (b) it opens up the possibility to integrate exfoliable materials into microwave circuitry. For these resonators, we observe the internal Q_i of $\approx 2 \times 10^4$ at 20 mK temperature and zero magnetic field. We study the magnetic field dependence of quality factor and resonance frequency dispersion of these resonators, primarily for two different thicknesses (t) of the NbN thin film. We find that Q_i is higher than 1000 for in-plane fields of ~ 1 T and perpendicular fields of ~ 100 mT. Few 100 mT is often the magnetic field range around which many materials show ferromagnetic, antiferromagnetic, and electron spin resonances.[34–36] For example, using average g-factor of 2.2 for chromium trihalides,[37] we find that approximately 160 mT magnetic field is required for resonant coupling of the magnons in these materials with microwave photons in a resonator with resonance frequency around 5 GHz. This makes NbN SCPW resonators an optimal platform for studying collective spin oscillations in different materials. Here we demonstrate coupling between a cavity mode in an NbN SCPW resonator and antiferromagnetic resonance (AFMR) modes in a chromium trichloride ($CrCl_3$) crystal — a van der Waals antiferromagnet.[34,36]

We use intrinsic silicon as substrate for fabrication of the SCPW resonators (we also fabricated resonators on sapphire substrate and the corresponding characterization data are included in the supplementary material). First, the wafers are spin-coated with a bilayer resist consisting of EL9 and PMMA 950 A2. Subsequently, the resonator pattern is made by electron beam lithography and developing in a solution of MIBK and IPA in 1:3 volume ratio. NbN is then deposited by reactive DC sputtering with a niobium (Nb) target at a sputtering power of 230 W in the presence of continuous flow of 11 sccm of nitrogen and 70 sccm of argon at a sputtering pressure of 6.5×10^{-3} mbar and temperature of 120 °C.[31] After sputtering, liftoff is done in acetone to remove the remaining resist along with the excess NbN film on top of them. On an NbN film of thickness 80 nm, transport measurements provide the following: $T_C \approx 12.5$ K, $H_C > 14$ T, RRR ≈ 0.9 and room temperature resistivity ≈ 1.95 μΩ m. Variation of resistivity with temperature for the NbN film on the intrinsic silicon substrate is shown in Fig. 1. The inset of Fig. 1 shows the SEM image of an NbN film where disorder is clearly visible.

The SCPW resonators are designed in a half-wave single port configuration. Figure 2(a) shows the SEM image of the device. The resonator has a trace width of 28 μm and has been designed from a section of coplanar waveguide with characteristic impedance of 46 Ω on intrinsic silicon, neglecting the surface impedance of the superconducting film. A coupling capacitor is made between input port and the resonator for coupling microwave power in-and-out of the resonator. The measurements are done in a dilution fridge, and a sufficient number of attenuators are kept at different plates of the fridge in the input line to ensure proper thermalization of microwave photons reaching the sample (more details in the supplementary material).
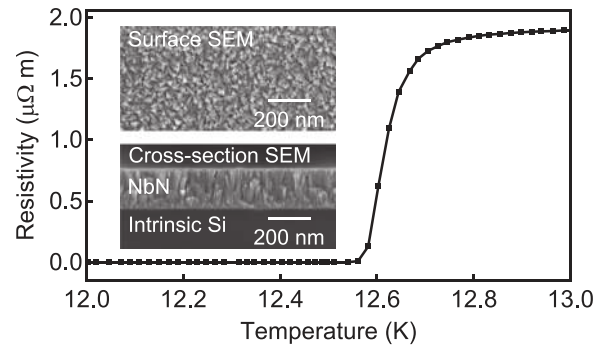
FIG. 1. Variation of resistivity of a 80 nm thick NbN film deposited by sputtering on intrinsic silicon with temperature (inset: SEM images of top and cross sectional views of an NbN film).

Ratio of reflected to input signal for a one-port capacitively coupled resonator in reflection geometry, as seen in Fig. 2(a), is described by the reflection coefficient S_{11}. Within the linear response of the resonator, S_{11} as a function of frequency, $f \left(= \frac{\omega}{2\pi}\right)$, for a half-wave single port resonator, can be modeled by

$$S_{11}(\omega) = 1 - \frac{Q_i}{\frac{1}{2}(Q_i + Q_e) + iQ_iQ_e\frac{\omega - \omega_0}{\omega_0}}, \quad (1)$$

where Q_i is the internal quality factor, Q_e is the external quality factor, and $f_0 \left(= \frac{\omega_0}{2\pi}\right)$ is the resonance frequency.[6] Figure 2(b) shows the representative measurement of the real part of S_{11} taken at 20 mK and
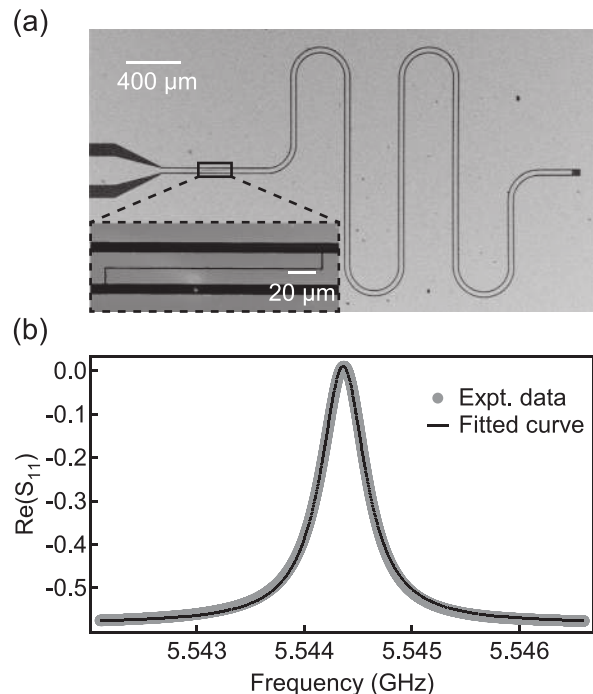
FIG. 2. (a) SEM image of an NbN SCPW resonator (inset: zoomed in image of coupling capacitor). (b) Real part of S_{11} measured at 20 mK temperature along with fitting function.

zero magnetic field, along with the fitted curve using Eq. (1). This allows us to extract the Q_i for various studies done in this work. We find maximum $Q_i \approx 22\,000$ at 20 mK temperature and zero magnetic field. We note that Q_e determines the coupling of the resonator to the external measurement circuitry. We have studied resonators which are designed to be overcoupled ($Q_i > Q_e$) and undercoupled ($Q_i < Q_e$) at base temperature and zero magnetic field to capture variation of Q_i in regimes with different internal loss rates. We have used the in-phase response (real part of S_{11}) to extract out the resonator parameters (details in the supplementary material).

As our primary motive is to develop these resonators for magnon coupling experiments,[35,38,39] it is imperative to characterize their response in magnetic field. Although the resonance frequency of a magnon mode depends on the geometry and the material properties, usually a magnetic field of ~ 100 mT could be sufficient to obtain magnon modes near 5 GHz.[34–36] Magnetic field dependence of the resonators in orientations parallel (B_{para}) and perpendicular (B_{perp}) to the SCPW plane has been shown in Fig. 3. Figures 3(a) and 3(b) show the color-scale plots of $|S_{11}|^2$ as a function of frequency and magnetic field for an NbN SCPW resonator, with a film thickness of 72 nm, on the
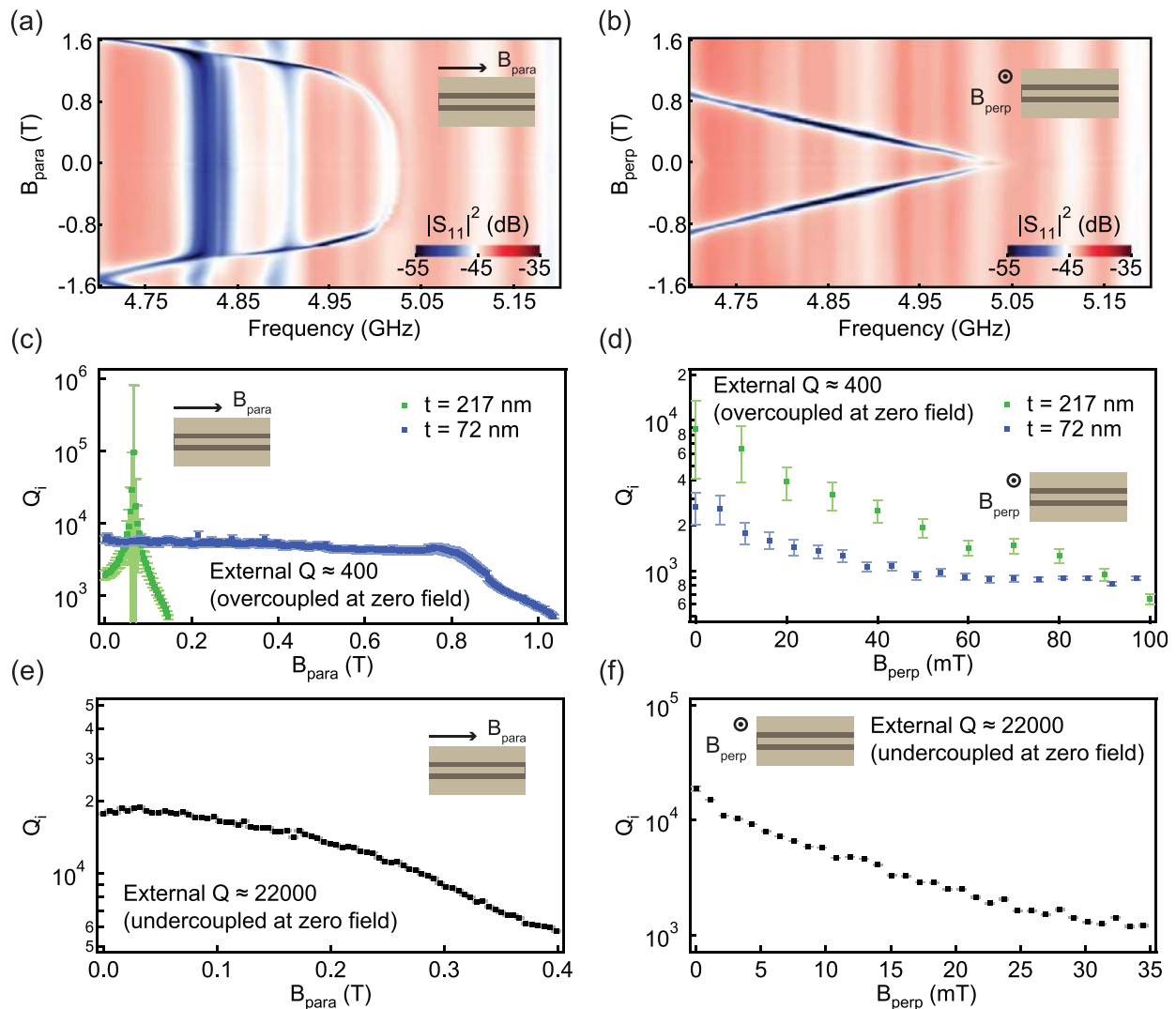
FIG. 3. Characterization of NbN resonators as a function of magnetic field. (a) and (b) Color-scale plots showing variation in $|S_{11}|^2$ for an NbN SCPW resonator with an NbN film thickness of 72 nm, with frequency and magnetic field for field orientations parallel and perpendicular to the SCPW plane, respectively. (c) and (d) Variation of Q_i with magnetic field for film thicknesses of 217 nm and 72 nm on the intrinsic silicon substrate, for parallel and perpendicular field orientations, respectively. These resonators are overcoupled, $Q_i \gg Q_e$, at zero magnetic field; Q_i reduces with increasing magnetic field due to vortex induced losses and eventually goes to the undercoupled regime, $Q_i < Q_e$; in undercoupled regime $|S_{11}|^2$ shows a dip at resonance frequency, while for $Q_i \gg Q_e$, change in $|S_{11}|^2$ is minimal. Although Q_i can be tracked up to large magnetic field range using this choice of Q_e, it gives rise to high error-bars in fits for Q_i when $Q_i \gg Q_e$ (near zero field). Another set of resonators with $Q_i \lesssim Q_e$ are studied to accurately determine Q_i near zero field. Dependencies at lower fields are more accurately calculated using these undercoupled resonators having a film thickness of 80 nm and are shown in (e) and (f) for parallel and perpendicular magnetic fields, respectively; here the error-bars have reduced to size comparable to the markers. Measurements were performed at 20 mK temperature.

intrinsic silicon substrate, for field orientations parallel and perpendicular to the SCPW plane. These measurements have been done in zero-field-cooled condition to address magnetic field induced losses while continuously varying magnetic field, as is required in many applications. Note that here the cavity is designed to be overcoupled at zero magnetic field. In the overcoupled regime, $|S_{11}|^2$ shows small variations (however, the resonance feature can be clearly seen in the phase response); hence, resonance dip is not visible at zero magnetic field. The dip starts appearing as vortex induced losses show up at higher fields.

Figures 3(c) and 3(d) show the Q_i values extracted from fit using Eq. (1) for resonators in magnetic field orientation parallel and perpendicular to the SCPW plane, respectively. Resonators in parallel field show a slower decrease in Q_i. This agrees with the fact that all the films have thicknesses below penetration depth, whereas, for perpendicular field, the rate of degradation of Q_i is much faster due to the dominant role of vortex dynamics induced losses over quasiparticle losses.[40]

Comparing the data for variation with magnetic field parallel to the SCPW plane, shown in Fig. 3(c) for 217 nm and 72 nm thick NbN films, we note that the degradation of Q_i is slower for the thinner film as dissipation due to vortex dynamics plays a lesser role and only quasiparticle losses are important; while for the thicker film this is not the case and there is an early onset of vortex dynamics induced losses. NbN films with smaller thicknesses maintain higher Q_i ($>10^3$) up to higher parallel magnetic field $B_{\text{para}} \approx 1$ T due to lower flux creep. For orientation of magnetic field perpendicular to the plane of the film, $Q_i > 10^3$ is observed up to $B_{\text{perp}} \approx 100$ mT field.

In Figs. 3(c) and 3(d), the resonators are overcoupled ($Q_i \gg Q_e$) at zero field. The choice of Q_e for this is good for tracking Q_i up to larger field range, but it leads to high error-bars in fits for Q_i in regime of low internal loss, which is realized near zero magnetic field. So, for determining Q_i more precisely in the low magnetic field regime, we fabricated another set of resonators with lower coupling capacitor such that $Q_i \lesssim Q_e$ at zero field. Figures 3(e) and 3(f) show the result of analysis for Q_i with this Q_e, and we notice that these results are consistent and have smaller fitting errors (additional details in the supplementary material).

The near quadratic and linear dispersion trends in Figs. 3(a) and 3(b), in orientations parallel and perpendicular to the magnetic field, respectively, are well described by Abrikosov-Gor'kov (AG) theory.[41] For SCPW resonators, the resonance frequency of the fundamental mode can be written as $f_0 = \frac{\beta}{\sqrt{L_l}}$, where $\beta = \frac{1}{2l\sqrt{C_l}}$ with l, C_l, and L_l being the length, capacitance per unit length, and inductance per unit length of the resonator. The total inductance contains contribution from the geometric inductance (L_g, per unit length) and the kinetic inductance (L_k, per unit length). As the shift in resonance frequency comes from the kinetic inductance part, it is straightforward to obtain $\frac{\Delta L_k}{L_k} = -\frac{2\beta^2}{\beta^2 - f_0^2 L_g} \frac{\Delta f_0}{f_{0,0}}$, where Δ represents change in associated quantity from its $B = 0$ T value (here Δf_0 is shift in resonance frequency from its value at base temperature and zero magnetic field, $f_{0,0}$). Now we use the fact that for $T \ll T_C$, $L_k \propto \frac{1}{T_C}$, and $k_B \Delta T_C = -\frac{\pi \alpha}{4}$, where α is the half of depairing energy and for a thin film in perpendicular magnetic field case, it can be written as $\alpha = DeB_{\text{perp}}$ where D is the the electronic diffusion constant and e is the magnitude of electron charge.[41,42] Using this formalism, we fit a straight line $\frac{\Delta f_0}{f_{0,0}} = -kB_{\text{perp}}$ to the dispersion (details in the supplementary material) and find D

from the relation $D = \frac{8k}{\pi e} \frac{\beta^2 k_B T_C}{\beta^2 - f_0^2 L_g}$. We find $D \approx 5 \times 10^{-4}$ m^{2}s^{-1} which is close to the values reported previously.[43]

We observe a weak hysteresis in the measurement depending on the sweep direction of the magnetic field (details in the supplementary material). All the measurements presented in Fig. 3 were recorded consistently with an upward sweep direction of the magnetic field. In parallel field orientation, a misalignment between the direction of the magnetic field and the plane of the superconducting film can also cause losses due to a non-zero out of plane component of the magnetic field. In our experiment, we estimated this misalignment to be less than 1° as the shift in resonant frequency remains flat for parallel magnetic field up to ≈ 0.8 T. We also characterized the resonators as a function of temperature and microwave power, and the details are provided in the supplementary material.

For application of the NbN SCPW resonators toward cavity magnonics devices, we investigated their coupling with magnons in CrCl$_3$ crystal, a van der Waals antiferromagnet. First, the microwave absorption spectroscopy of CrCl$_3$ was performed using a 20–30 μm thick CrCl$_3$ crystal flake placed on a coplanar waveguide type transmission line made out of copper on a printed circuit board (PCB) (measurement setup shown in supplementary material). The crystal was transferred to the PCB inside a glovebox and covered with Apeizon N grease to protect against ambient. This measurement was done in a cryostat under continuous flow of helium vapor at a temperature of 1.5 K. On applying a magnetic field oriented parallel to the plane of the PCB and perpendicular to the direction of RF current in the transmission line, we observe two symmetry protected antiferromagnetic resonance modes in the presence of a mode-crossing in the transmission spectra as shown in Fig. 4(a). The linearly dispersing mode (f_1) has been identified as the acoustic mode and the downward-going mode (f_2) has been identified as the optical mode. The two modes get excited when certain symmetry rules are satisfied. These modes and the symmetry arguments have been studied in detail in Refs. 34 and 36. In our experiments, the DC magnetic field is always applied in the plane of the sample and perpendicular to the direction of the RF current.[34,36] Using the derivative divide method,[44] the data in Fig. 4(a) have been analyzed, and the linewidth of the acoustic and optical modes has been determined as $\frac{\gamma_1}{2\pi} \approx 0.33$ GHz and $\frac{\gamma_2}{2\pi} \approx 0.42$ GHz, respectively. The variation in these linewidths with magnetic field is found to be small.[36] We note that the optical mode has a broader linewidth compared to the acoustic mode.

After this, we placed a similar crystal flake at the current antinode of the NbN resonator on an intrinsic Si chip inside glovebox and similarly covered with Apeizon N grease. This measurement was done in the dilution fridge, and the grease provided additional benefit of good thermal anchoring of the crystal to the 20 mK plate temperature. On applying magnetic field parallel to the SCPW plane and perpendicular to the RF current direction at the current antinode, we observe formation of avoided crossing between the cavity mode and each of the two AFMR modes in the measured $|S_{11}|^2$, as shown in Fig. 4(b). This is the signature of strong magnon-photon coupling between microwave photons in the NbN resonator and antiferromagnetic magnons in CrCl$_3$. Figure 4(c) shows line-plots at different magnetic fields. Frequency dispersion of the modes in Fig. 4(b) and broader linewidth of the hybrid mode associated with the optical AFMR mode in Fig. 4(c) agree with the results from the transmission spectroscopy measurement using the copper transmission line.
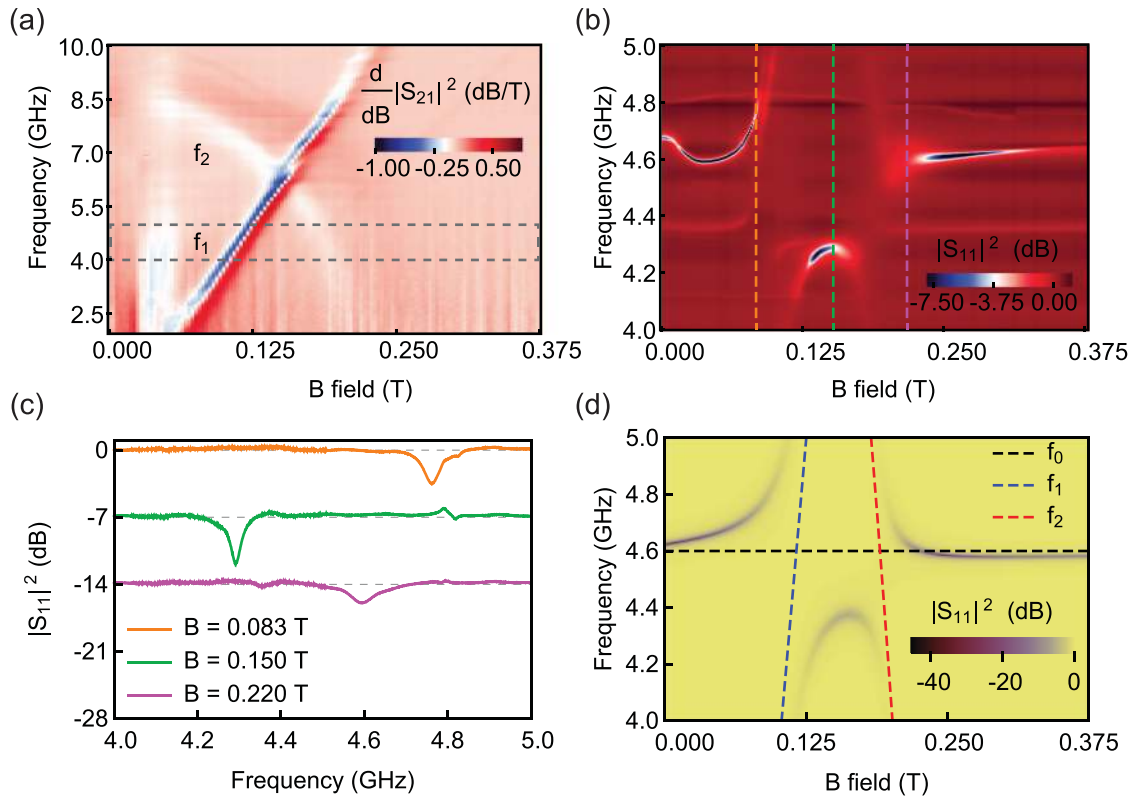
FIG. 4. Strong coupling between magnon modes in $CrCl_3$ and photon mode in NbN resonator. (a) Transmission spectra showing magnetic field dispersion of acoustic (f_1) and optical (f_2) AFMR modes in a $CrCl_3$ crystal flake placed on a copper coplanar waveguide transmission line. (b) Color-scale plot of the normalized $|S_{11}|^2$ with magnetic field and frequency for a $CrCl_3$ crystal flake placed at the current antinode of an NbN SCPW resonator. The plot range is same as the gray dashed rectangle in (a) and shows the hybridization of the cavity mode with the acoustic and optical AFMR modes in $CrCl_3$ due to strong magnon-photon coupling. (c) Line-plots at three different fields (corresponding to dashed lines of same color in (b)). Offset of -7 dB has been added in consecutive plots for clarity. Line-shapes of upper hybrid modes, formed due to hybridization of cavity mode with acoustic and optical AFMR modes (orange and magenta, respectively), agree with the relatively broader linewidth of optical mode compared to acoustic mode, as apparent from (a). (d) Plot of calculated $|S_{11}|^2$ using input–output theory with coupling strength of acoustic and optical AFMR modes with cavity mode of 0.57 GHz and 0.37 GHz, respectively (dashed lines show the bare cavity (f_0), acoustic (f_1) and optical (f_2) AFMR modes).

We further generated a plot of $|S_{11}|^2$ from the calculation based on input-output theory.[14,45,46] According to this theory, the reflection coefficient (S_{11}) for the system with two non-interacting magnon modes coupled with a cavity photon mode can be written as

$$S_{11}(\omega) = 1 - \cfrac{\kappa_e}{i(\omega - \omega_0) + \cfrac{\kappa_i + \kappa_e}{2} + \cfrac{|g_1|^2}{i(\omega - \omega_1) + \cfrac{\gamma_1}{2}} + \cfrac{|g_2|^2}{i(\omega - \omega_2) + \cfrac{\gamma_2}{2}}},$$
(2)

where $\kappa_i = \frac{\omega_0}{Q_i}$ and $\kappa_e = \frac{\omega_0}{Q_e}$, $\frac{\omega_1}{2\pi} = f_1$ and $\frac{\omega_2}{2\pi} = f_2$ are the field dependent resonance frequencies of the acoustic and optical magnon modes, respectively, $\frac{\gamma_1}{2\pi}$ and $\frac{\gamma_2}{2\pi}$ are their linewidths, and $\frac{g_1}{2\pi}$ and $\frac{g_2}{2\pi}$ are their coupling strength with the cavity mode, respectively. For fitting the mode-coupling data shown in Fig. 4(b), we defined a three mode coupling Hamiltonian matrix. The diagonal elements of this symmetric matrix comprises of the bare cavity mode, the bare acoustic magnon mode, and the bare optical magnon mode. We keep the off-diagonal terms representing the coupling between cavity and acoustic mode, and

between cavity and optical mode as fitting parameters, and take the cross coupling term between the two magnon modes to be zero. The field dependence of the acoustic and the optical modes was obtained from polynomial fits to the bare magnon modes data shown in Fig. 4(a), and the cavity mode was assumed to be constant in the field range considered. We use the field dependent functional forms of the eigenmodes of this matrix to perform a non-linear model fitting to the experimentally obtained mode-coupling data shown in Fig. 4(d). This fitting gives $\frac{g_1}{2\pi} = 0.57$ GHz and $\frac{g_2}{2\pi} = 0.37$ GHz. Using these g values, we obtain the plot as shown in Fig. 4(d) with the expression from input-output theory Eq. (2). The calculated cooperativity of coupling between acoustic magnon and photon, and between optical magnon and photon, using these values is $C_1 = \frac{g_1^2}{\kappa \gamma_1} = 47.10$ and $C_2 = \frac{g_2^2}{\kappa \gamma_2} = 15.59$, respectively, where $\kappa = \kappa_i + \kappa_e$. The cooperativities larger than the expected modes occupancy clearly suggest a quantum-coherent coupling between the photons and the magnons.

Since we use a $CrCl_3$ crystal covering almost the entire SCPW resonator, the effective volume for magnon-photon coupling is determined mainly by the magnetic mode volume of the resonator. From

the lattice structure parameters of $CrCl_3$ and using the magnetic component of the vacuum RF field of the resonator,[38,47] we calculate the coupling strength per spin to be $\frac{g_0}{2\pi} \approx 7.93$ Hz and a net coupling strength of ≈ 1.09 GHz for the estimated effective volume (more details regarding fitting and g value estimation is provided in the supplementary material). The deviation in the estimated and experimentally measured coupling rates could be attributed to reduction in the effective volume as predominantly the spins near the gap of resonator contribute to the measured signal. Also, coupling strength for the acoustic and the optical modes separately depend on both geometry and symmetry, as we observe them to be. A more accurate microscopic calculation and further experiments are needed to fully understand some aspects of the mode coupling data. This can be a focus of our future work. We also observe a faint dispersing mode below the main cavity mode in Fig. 4(b) which also couples with the AFMR modes. This is possibly a parasitic mode of the resonator whose origin needs to be verified. Furthermore, a slight downward shift in cavity frequency with increasing magnetic field, seen between 10 mT and 30 mT, could possibly be attributed to the change in magnetic state of $CrCl_3$ as it undergoes spin-flop transition.[48–50] This measurement shows that our NbN resonators can be an ideal platform for studying collective spin oscillations and their coupling with electromagnetic modes of microwave frequencies in different systems.

In this work, we have fabricated NbN SCPW resonators using a simple fabrication process and probed their baseline properties. We see $Q_i > 10^3$ persisting up to perpendicular magnetic field of 100 mT, which is two times higher than the previously reported results.[30] Using substrate surface treatments and vortex trapping schemes, Q_i of these resonators can be made even higher with better performance possibly up to even higher magnetic fields. Our fabrication protocols have the potential to incorporate exfoliable crystals in the microwave circuits. Furthermore, we have demonstrated the effectiveness of these resonators in coupling with spin ensembles by coupling them to magnons in a van der Waals antiferromagnetic system to study collective spin oscillations and making hybrid quantum devices.

See the supplementary material for details on measurement circuit, fitting procedure along with comparison between overcoupled and undercoupled resonators, characterization data for resonators on the intrinsic silicon and sapphire substrate with temperature and microwave power, and details about the magnon-photon coupling experiment.

AUTHORS' CONTRIBUTIONS

Su.M. and L.N.K. contributed equally to this work.

DATA AVAILABILITY

The data that support the findings of this study are available from the corresponding author upon reasonable request.

REFERENCES

[1]P. K. Day, H. G. LeDuc, B. A. Mazin, A. Vayonakis, and J. Zmuidzinas, Nature **425**, 817 (2003).

[2]E. A. Tholén, A. Ergül, E. M. Doherty, F. M. Weber, F. Grégis, and D. B. Haviland, Appl. Phys. Lett. **90**, 253509 (2007).

[3]M. A. Castellanos-Beltran and K. W. Lehnert, Appl. Phys. Lett. **91**, 083509 (2007).

[4]A. Wallraff, D. I. Schuster, A. Blais, L. Frunzio, R.-S. Huang, J. Majer, S. Kumar, S. M. Girvin, and R. J. Schoelkopf, Nature **431**, 162 (2004).

[5]C. A. Regal, J. D. Teufel, and K. W. Lehnert, Nat. Phys. **4**, 555 (2008).

[6]V. Singh, S. J. Bosman, B. H. Schneider, Y. M. Blanter, A. Castellanos-Gomez, and G. A. Steele, Nat. Nanotechnol. **9**, 820 (2014).

[7]Y. Kubo, F. R. Ong, P. Bertet, D. Vion, V. Jacques, D. Zheng, A. Dréau, J.-F. Roch, A. Auffeves, F. Jelezko, J. Wrachtrup, M. F. Barthe, P. Bergonzo, and D. Esteve, Phys. Rev. Lett. **105**, 140502 (2010).

[8]R. Amsüss, C. Koller, T. Nöbauer, S. Putz, S. Rotter, K. Sandner, S. Schneider, M. Schramböck, G. Steinhauser, H. Ritsch, J. Schmiedmayer, and J. Majer, Phys. Rev. Lett. **107**, 060502 (2011).

[9]V. Ranjan, G. de Lange, R. Schutjens, T. Debelhoir, J. P. Groen, D. Szombati, D. J. Thoen, T. M. Klapwijk, R. Hanson, and L. DiCarlo, Phys. Rev. Lett. **110**, 067004 (2013).

[10]A. Tkalcec, S. Probst, D. Rieger, H. Rotzinger, S. Wünsch, N. Kukharchyk, A. D. Wieck, M. Siegel, A. V. Ustinov, and P. Bushev, Phys. Rev. B **90**, 075112 (2014).

[11]C. W. Zollitsch, K. Mueller, D. P. Franke, S. T. B. Goennenwein, M. S. Brandt, R. Gross, and H. Huebl, Appl. Phys. Lett. **107**, 142105 (2015).

[12]J. R. Petta, A. C. Johnson, J. M. Taylor, E. A. Laird, A. Yacoby, M. D. Lukin, C. M. Marcus, M. P. Hanson, and A. C. Gossard, Science **309**, 2180 (2005).

[13]K. C. Nowack, F. H. L. Koppens, Y. V. Nazarov, and L. M. K. Vandersypen, Science **318**, 1430 (2007).

[14]D. I. Schuster, A. P. Sears, E. Ginossar, L. DiCarlo, L. Frunzio, J. J. L. Morton, H. Wu, G. A. D. Briggs, B. B. Buckley, D. D. Awschalom, and R. J. Schoelkopf, Phys. Rev. Lett. **105**, 140501 (2010).

[15]H. Malissa, D. I. Schuster, A. M. Tyryshkin, A. A. Houck, and S. A. Lyon, Rev. Sci. Instrum. **84**, 025116 (2013).

[16]O. W. B. Benningshof, H. R. Mohebbi, I. A. J. Taminiau, G. X. Miao, and D. G. Cory, J. Magn. Reson. **230**, 84 (2013).

[17]F. E. Schmidt, M. D. Jenkins, K. Watanabe, T. Taniguchi, and G. A. Steele, Nat. Commun. **9**(1), 4069 (2018).

[18]J. G. Kroll, W. Uilhoorn, K. L. van der Enden, D. de Jong, K. Watanabe, T. Taniguchi, S. Goswami, M. C. Cassidy, and L. P. Kouwenhoven, Nat. Commun. **9**(1), 064053 (2018).

[19]J. I.-J. Wang, D. Rodan-Legrain, L. Bretheau, D. L. Campbell, B. Kannan, D. Kim, M. Kjaergaard, P. Krantz, G. O. Samach, F. Yan, J. L. Yoder, K. Watanabe, T. Taniguchi, T. P. Orlando, S. Gustavsson, P. Jarillo-Herrero, and W. D. Oliver, Nat. Nanotechnol. **14**, 120 (2019).

[20]C. Gong and X. Zhang, Science **363**, eaav4450 (2019).

[21]V. Singh, B. H. Schneider, S. J. Bosman, E. P. J. Merkx, and G. A. Steele, Appl. Phys. Lett. **105**, 222601 (2014).

[22]V. E. Calado, S. Goswami, G. Nanda, M. Diez, A. R. Akhmerov, K. Watanabe, T. Taniguchi, T. M. Klapwijk, and L. M. K. Vandersypen, Nat. Nanotechnol. **10**, 761 (2015).

[23]D. J. van Woerkom, A. Geresdi, and L. P. Kouwenhoven, Nat. Phys. **11**, 547 (2015).

[24]M. R. Vissers, J. Gao, D. S. Wisbey, D. A. Hite, C. C. Tsuei, A. D. Corcoles, M. Steffen, and D. P. Pappas, Appl. Phys. Lett. **97**, 232509 (2010).

[25]F. W. Carter, T. Khaire, C. Chang, and V. Novosad, Appl. Phys. Lett. **115**, 092602 (2019).

[26]C. Song, T. W. Heitmann, M. P. DeFeo, K. Yu, R. McDermott, M. Neeley, J. M. Martinis, and B. L. T. Plourde, Phys. Rev. B **79**, 174512 (2009).

[27]A. Ghirri, C. Bonizzoni, D. Gerace, S. Sanna, A. Cassinese, and M. Affronte, Appl. Phys. Lett. **106**, 184101 (2015).

[28]C. Song, M. P. DeFeo, K. Yu, and B. L. T. Plourde, Appl. Phys. Lett. **95**, 232501 (2009).

[29]D. Bothner, T. Gaber, M. Kemmler, D. Koelle, and R. Kleiner, Appl. Phys. Lett. **98**, 102504 (2011).

[30]J. Kroll, F. Borsoi, K. van der Enden, W. Uilhoorn, D. de Jong, M. Quintero-Pérez, D. van Woerkom, A. Bruno, S. Plissard, D. Car, E. Bakkers, M. Cassidy, and L. Kouwenhoven, Phys. Rev. Appl. **11**, 064053 (2019).

[31]S. P. Chockalingam, M. Chand, J. Jesudasan, V. Tripathi, and P. Raychaudhuri, Phys. Rev. B **77**, 214503 (2008).

[32]M. Mondal, A. Kamlapure, M. Chand, G. Saraswat, S. Kumar, J. Jesudasan, L. Benfatto, V. Tripathi, and P. Raychaudhuri, Phys. Rev. Lett. **106**, 047001 (2011).

[33]A. Kamlapure, M. Mondal, M. Chand, A. Mishra, J. Jesudasan, V. Bagwe, L. Benfatto, V. Tripathi, and P. Raychaudhuri, Appl. Phys. Lett. **96**, 072509 (2010).

[34]D. MacNeill, J. T. Hou, D. R. Klein, P. Zhang, P. Jarillo-Herrero, and L. Liu, Phys. Rev. Lett. **123**, 047204 (2019).

[35]X. Zhang, C.-L. Zou, L. Jiang, and H. X. Tang, Phys. Rev. Lett. **113**, 156401 (2014).

[36]L. N. Kapoor, S. Mandal, P. C. Adak, M. Patankar, S. Manni, A. Thamizhavel, and M. M. Deshmukh, Adv. Mater. 2005105 (published online, 2020).

[37]H. H. Kim, B. Yang, S. Li, S. Jiang, C. Jin, Z. Tao, G. Nichols, F. Sfigakis, S. Zhong, C. Li, S. Tian, D. G. Cory, G.-X. Miao, J. Shan, K. F. Mak, H. Lei, K. Sun, L. Zhao, and A. W. Tsen, Proc. Natl. Acad. Sci. U. S. A. **116**, 11131 (2019).

[38]H. Huebl, C. W. Zollitsch, J. Lotze, F. Hocke, M. Greifenstein, A. Marx, R. Gross, and S. T. B. Goennenwein, Phys. Rev. Lett. **111**, 127003 (2013).

[39]Y. Tabuchi, S. Ishino, T. Ishikawa, R. Yamazaki, K. Usami, and Y. Nakamura, Phys. Rev. Lett. **113**, 083603 (2014).

[40]S. Kwon, A. Fadavi Roudsari, O. W. B. Benningshof, Y.-C. Tang, H. R. Mohebbi, I. A. J. Taminiau, D. Langenberg, S. Lee, G. Nichols, D. G. Cory, and G.-X. Miao, J. Appl. Phys. **124**, 033903 (2018).

[41]M. Tinkham, *Introduction to Superconductivity*, Dover Books on Physics Series (Dover Publications, 2004).

[42]N. Samkharadze, A. Bruno, P. Scarlino, G. Zheng, D. P. DiVincenzo, L. DiCarlo, and L. M. K. Vandersypen, Phys. Rev. Appl. **5**, 044004 (2016).

[43]M. Mondal, A. Kamlapure, S. C. Ganguli, J. Jesudasan, V. Bagwe, L. Benfatto, and P. Raychaudhuri, Sci. Rep. **3**, 1357 (2013).

[44]H. Maier-Flaig, S. T. B. Goennenwein, R. Ohshima, M. Shiraishi, R. Gross, H. Huebl, and M. Weiler, Rev. Sci. Instrum. **89**, 076101 (2018).

[45]E. Abe, H. Wu, A. Ardavan, and J. J. L. Morton, Appl. Phys. Lett. **98**, 251108 (2011). publisher: American Institute of Physics.

[46]A. A. Clerk, M. H. Devoret, S. M. Girvin, F. Marquardt, and R. J. Schoelkopf, Rev. Mod. Phys. **82**, 1155 (2010).

[47]N. J. Lambert, J. A. Haigh, and A. J. Ferguson, J. Appl. Phys. **117**, 053910 (2015).

[48]A. Narath and H. L. Davis, Phys. Rev. **137**, A163 (1965).

[49]M. A. McGuire, G. Clark, S. Kc, W. M. Chance, G. E. Jellison, V. R. Cooper, X. Xu, and B. C. Sales, Phys. Rev. Mater. **1**, 014001 (2017).

[50]B. Kuhlow, Phys. Status Solidi A **72**, 161 (1982).